Silicon pixel detector for the TTF-FEL beam trajectory monitor

J.S.T. Ng[a,*], P. Holl[b], K. Hansen[a], J. Kemmer[b], P. Lechner[b],
U.C. Müller[a], L. Strüder[c]

[a]*Deutsches Elektronen-Synchrotron DESY, Notkestr. 85, D-22603 Hamburg, Germany*
[b]*Ketek GmbH, Am Isarbach 30, D-85764 Oberschleißheim, Germany*
[c]*Max-Planck-Institut für extraterrestrische Physik, Giessenbachstraße, D-85740 Garching, Germany*

Abstract

In order to achieve the high brightness promised by the single-pass Free Electron Laser (FEL) at the TESLA Test Facility (TTF) at DESY, the electron beam position must be controlled better than 10 μm over a distance of 15 m. The design of a monitor system with this accuracy is described. The silicon pixel detector, which is critical to this monitor, must have a position resolution of 1 μm and an excellent sensitivity for soft X-rays above 150 eV. The silicon pixel detector and its readout electronics are also described.

1. Introduction

A free electron laser operating in the Self-Amplified Spontaneous Emission (SASE) regime could provide coherent radiation with brightness far exceeding those of the current generation of synchrotron radiation light sources. In a SASE-FEL, the electron beam passes through a long undulator and interacts with its own spontaneous radiation. This interaction is a pre-requisite for lasing. Any significant deviation in the electron beam from a straight trajectory must be detected and corrected to allow for overlap with the photon beam. At the TTF-FEL under construction at DESY, the electron beam from a superconducting linear accelerator will have an energy of 300–500 MeV in the initial stage, and the FEL first harmonic wavelength will be 25–70 nm [1]. The undulator beam line is 15 m long with a beam pipe inner diameter of ~ 10 mm. In order to achieve a SASE efficiency of more than 90%, the average electron trajectory deviation must be less than 10 μm over a 15 m distance.

In the beam trajectory monitor [2], the off-axis spontaneous undulator radiation is detected through a set of pinholes by high resolution silicon pixel detectors as shown in Fig. 1. The two pinhole positions and the corresponding pair of measured image points define two lines which are constrained
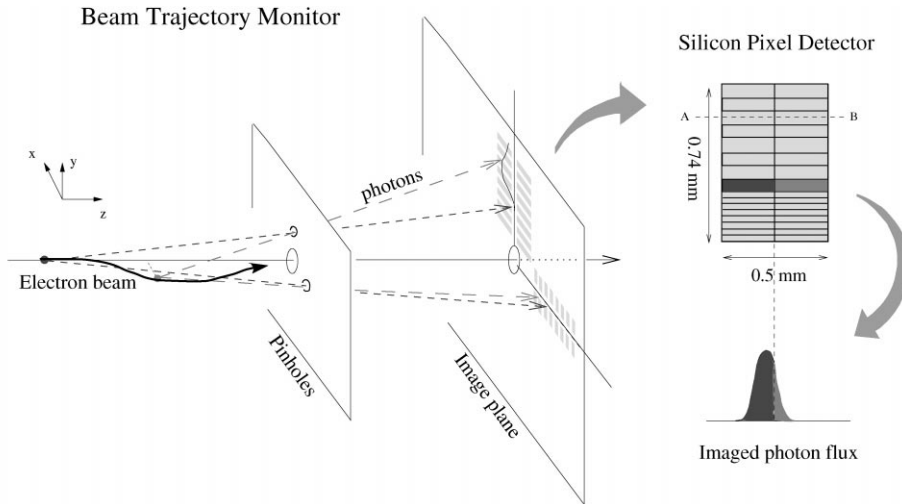
Fig. 1. An overview of the beam trajectory monitor system.

to the same source point, and are used to reconstruct the beam trajectory. The centroid of the photon flux through the pinhole is measured by the relative signal in a pair of pixels with 1 μm resolution which corresponds to a 10 μm transverse beam displacement. The longitudinal beam position is determined by the radial coordinate of the image given by the pixel segmentation and is limited to a resolution in the range of 0.5 m to 2.5 m by diffraction broadening of the image through the pinhole. A thin (0.25 μm) silver foil is used to suppress the flux of photons below 150 eV (8 nm) in order to minimize the effect of diffraction. There will be one such trajectory monitor system at the end of each 5 m long undulator module along the beam line.

2. Detector and readout requirements

The space available for the detectors is limited and the required position resolution is quite stringent, so silicon pixel detectors are considered. The position resolution is determined by the signal-to-noise ratio, therefore the detector must have low noise and an excellent sensitivity to Vacuum Ultra-Violet (VUV) radiation. Also, a fabrication technology that leads to a uniform and thin back-

entrance window should be used because the absorption length for photons with 150 eV energy is only 50 nm in silicon.

The angular distribution of the undulator radiation is quite complicated [2]. The photon flux changes by more than three orders of magnitude over the angular acceptance of the pixel detector. Therefore, the readout electronics should be flexible and allow for each pixel-pair to accumulate sufficient photon signal. The beam bunches are separated by 111 ns. The number of bunches to be gated vary from 6 to 2500 for the pixels closest to the beam to the ones furthest away. The corresponding integration time then varies from 0.5 to 300 μs. The electronics must not contribute excess noise under this condition.

The monitor system provides a well-defined optical axis because the pixel response can be accurately calibrated with a laser line-source. This calibration is to be maintained by precision charge injection, both directly onto the pixels and at the input to the frontend electronics.

3. Pixel detector layout

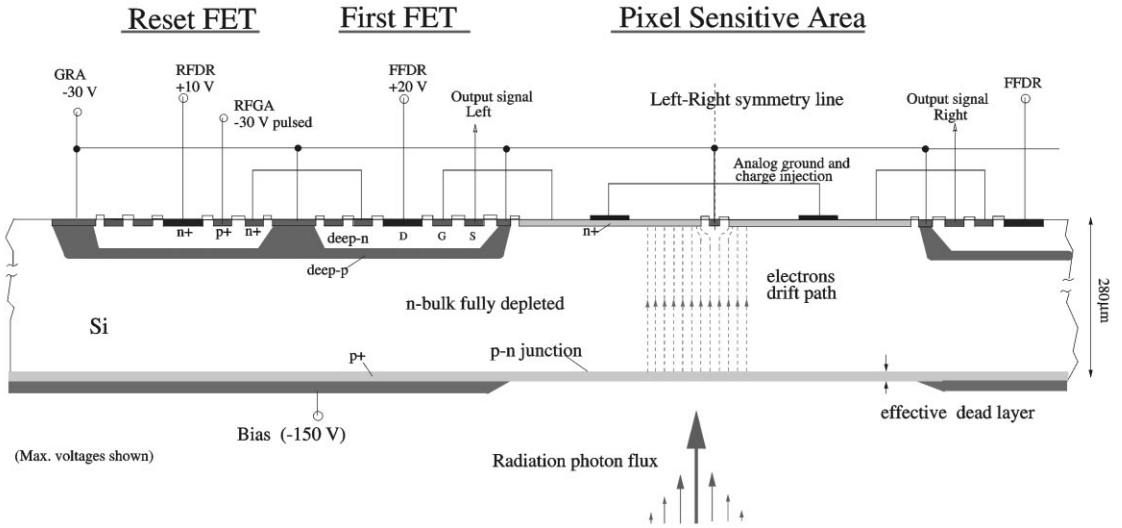A rough sketch of the top view of the pixel detector is already shown in Fig. 1. Each detector

Fig. 2. A cross section of the pixel detector. It is a cut along the dash line AB in Fig. 1. See text for details.

chip is 4.1 mm × 2.5 mm. There are two columns of pixels with a total of 24 outputs. The pixel length is 250 μm; the width varies from 25 (nearest to the beam) to 100 μm to partially account for the rapidly changing photon flux and viewing angle. Because of the need to place the detector near the beam, the first active pixel is only 1 mm from the edge of the chip. Each pixel is directly connected to an on-chip JFET; a second JFET resets the charge after each readout cycle. The JFETs are integrated next to the pixels using single sided n-channel technology [3], allowing to take advantage of the low pixel capacitance for low noise performance. The minimum size of the JFET is 50 μm, and only every other 25 μm wide pixel is read out. The non-readout pixels are biased to the same potential as the readout ones by an additional metal strip. The same strip is realized as a MOS structure over all readout pixels. It can be used to simultaneously test-pulse all pixels with coupling capacitance of approximately 144 fF. The relative accuracy due to the fabrication process is better than 0.1% for the left/right pixels.

Note: the arrangement of readout and non-readout pixels should not be confused with a method for strip detectors, where capacitively coupled strips enhance the position resolution.

Here the non-readout pixels are held at a fixed potential and cannot couple a signal to their neighbors. The aim is to reduce the effective sensitive area and limit the data rate to an acceptable level in that part of the detector where the photon flux is highest.

Some details of the pixel detector design can be seen from the cross-section view shown in Fig. 2. The silicon bulk is n-type, 280 μm thick, 4 kΩ-cm. On one surface of the chip, the pixels are formed by n^+-implants and isolated from each other by a 5 μm wide p^+ grid. The active area of the device can be fully depleted by a 2×1 mm^2 p–n junction on the reverse side. Moreover, this p–n junction is optimized for the detection of low-energy photons. The quantum efficiency is more than 50% in the range from 100 eV to 10 keV [4]. This corresponds to an effective dead layer of ~ 30 nm. The extent of the structure was derived from 2D simulations to ensure a uniform drift field in the pixel region.

4. Front-end electronics

Each pixel output signal is connected to one channel of the CAMEX64B [5]. This JFET-CMOS chip provides signal amplification, noise filtering
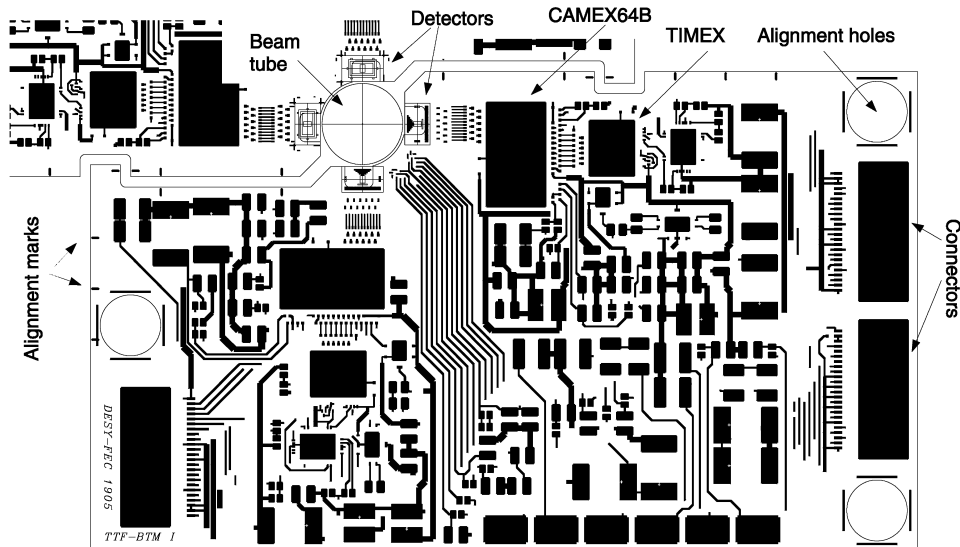
Fig. 3. Layout of the hybrid board in the beam pipe region, showing the detector mounting scheme and the connection to frontend electronics.

using switched capacitors with double-correlated sampling, and multiplexed output of up to 64 channels. A digital steering chip (TIMEX) is used to generate the necessary control signals, reducing the number of input lines to only three (clock, timing, and initialization). The timing sequence can be easily programmed for each chip and a variety of integration duration can be realized for each detector. The power consumption can go up to 0.55 W per chip, and since the complete detector assembly is to be operated in ultra-high vacuum to measure VUV photons, a thermoelectric cooler is needed to remove the heat. (This also allows cooling the detectors down to $-10°C$ for better noise performance.)

5. Hybrid board

The ceramic hybrid board provides the platform for mounting the detector and frontend chips, realization of multilayer circuits, and support for the Peltier cooler. One complete hybrid with two detectors and portion of a complementary one is shown in Fig. 3. The detector is bonded on both sides, the back side for the depletion bias voltage and the front side for the JFET supplies, charge injection, and signal outputs. An upper layer circuit is realized with gold traces on the 635 μm thick Al_2O_3 board while a lower single layer is realized on the back-side [6]. Through-vias 100–200 μm wide are used to bring all lines to the top surface, which are then connected to the outside using flexible foils. The circuit provides filtering and distribution of power lines, differential receivers for the digital signals, and a driver for the outputs.

Because of the small detector chip size and the need to leave open the back-entrance window, gluing is only possible on two edges, one 0.5 mm and the other 1 mm wide. The nearest gluing edge to the window is 400 μm, while the minimum distance between the hybrid and the beam pipe is 185 μm. The resulting dimension tolerance of ± 50 μm for the ceramic board can be achieved with high precision laser cutting technique [6]. The same technique is used to drill holes for precision alignment pins. Because the thermal conductivity of Al_2O_3 is relatively good, and the 35 μm Al_2O_3 insulation layer is sufficiently thin, the Peltier cooler can be mounted on the back-side, underneath the

CAMEX64B chip which is the main heat source. Test measurements also show that Al_2O_3 has excellent out-gassing properties and is compatible with ultra-high vacuum.

6. Expected performance

The photon flux centroid position is determined by using a non-linear interpolation of the signals measured in two pixels [7]. The fractional error in the photon signal measurement in each pixel, including electronics noise and fluctuations in the electron–hole pair creation and charge collection processes, as well as fluctuation in the photon flux, is

$$\left(\frac{\delta S}{S}\right)^2 = \left(\frac{\text{ENC}}{S}\right)^2 + \frac{1}{N_\gamma}\left[1 + \frac{1}{\alpha}\left(F + \frac{1}{\varepsilon}\right)\right] \qquad (1)$$

where ENC is the noise charge at the preamplifier input, N_γ the number of photons in each pixel, F the Fano factor, ε the quantum efficiency, and $\alpha = E_\gamma/w$ where E_γ is the photon energy, w the electron–hole pair creation energy. Assuming a Gaussian distributed photon flux with RMS width σ centered between the two pixels, the error in the position given by the charge sharing method is

$$\delta x = \frac{\sqrt{\pi}}{2}\left(\frac{\delta S}{S}\right)\sigma, \qquad (2)$$

where $\sigma \sim 100$ μm as given by the pinhole size and the effects of diffraction. The position error is dominated by the fluctuation in the photon signal. For $\delta x \sim 1$ μm, the required signal and noise figures $N_\gamma \sim 1000$ and ENC ~ 300 e can be achieved.

A detailed simulation to study the trajectory reconstruction and correction has also been carried out [8]. It includes calculation of the undulator radiation, alignment errors in the quadrupoles (± 50 μm), errors in the undulator magnet dipoles (0.1%), and systematic effects due to beam optics (finite widths in the electron beam size and angle, and the divergence/convergence effects of the FODO lattice). The deviation from a straight trajectory in the electron beam is then reconstructed using this monitor. A simple correction algorithm is used, which finds the best setting for the steering corrector magnets to bring the measured point back to nominal beam axis, one at a time along the trajectory. The average deviation is typically 88 μm before correction, and reduces to 8 μm after correction.

7. Summary

A silicon pixel detector with 1 μm position resolution for soft X-rays has been designed for the TTF-FEL beam trajectory monitor, and is currently being produced. With this monitor, the optical axis for the electron beam is defined precisely by one single system over a distance of 6 m for the present design. The required alignment and fabrication precision is challenging. The system is under construction and test results are expected in the near future.

References

[1] TTF-FEL Conceptual Design Report, TESLA-FEL 95-03, DESY, June 1995; J. Rossbach et al., Nucl. Instr. and Meth. A 375 (1996) 269.
[2] J.S.T. Ng, TESLA-FEL 96-16, DESY, 1996; R. Bonifacio, W.A. Barletta (Eds.), AIP Conference Proceedings #413, 1997.
[3] P. Rehak et al., Nucl. Instr. and Meth. A 288 (1990) 168.
[4] H. Soltau et al., Nucl. Instr. and Meth. A 377 (1996) 340.
[5] W. Buttler, G. Lutz et al., Nucl. Instr. and Meth. A 288 (1990) 140.
[6] A. Gandi et al., CERN EST/SM group, Geneva, Switzerland.
[7] E. Belau et al., Nucl. Instr. and Meth. 214 (1983) 253.
[8] U.C. Müller, in: R. Bonifacio, W.A. Barletta (Eds.), AIP Conference Proceedings #413: Workshop on High Gain FELs, Garda Lake, 1997.